

6.7 WHITECAP FRACTION OF ACTIVELY BREAKING WAVES: TOWARD A DATABASE APPLICABLE FOR DYNAMIC PROCESSES IN THE UPPER OCEAN

Magdalena D. Anguelova and Paul A. Hwang

Remote Sensing Division, Naval Research Laboratory, 20375, Washington DC, USA
Telephone: 202-404-6342; E-mail: maggie.anguelova@nrl.navy.mil

1. INTRODUCTION

Oceanic whitecaps are the most direct surface expression of breaking wind waves in the ocean. Whitecap fraction W quantifies the breaking events and is thus a suitable forcing variable for parameterizing and predicting air-sea interaction processes affected by breaking waves. Whitecaps are dynamic features on the ocean surface which evolve quickly (Callaghan et al., 2012), and thus have markedly different properties in different lifetime stages. At the moment of active breaking, the whitecaps are thick, comprise wide range of bubble sizes, move along with the wave crest, and cover less surface area. We refer to this actively generated sea foam as active whitecaps, aka stage A (young) whitecaps (Monahan and Woolf, 1989). In contrast, the foam decaying after the breaking event and the froth formed by the bubbles rising from below are thinner, linger almost motionless behind the wave that has created them, and spread over a larger area. We refer to these decaying foam patches as residual whitecaps, aka stage B (mature) whitecaps.

Both active and residual whitecaps contribute to the total value W , with their relative contributions depending on the wind speed and other meteorological and environmental factors. While W could be associated with some air-sea processes, e.g., bubble-mediated sea spray production and heat exchange (Andreas et al., 2008; de Leeuw et al., 2011), many other, more dynamical air-sea processes must be represented in terms of active whitecap fraction W_A , e.g., production of spume droplets (important for the intensification of tropical storms), momentum flux, turbulent mixing, gas exchange, and generation of ambient noise in the ocean (Melville, 1996; Asher et al., 1998; Andreas et al., 2008).

Photographic measurements of whitecap fraction often quantify W without clear measure of the contributions of active and residual whitecaps (Monahan et al., 1983; Stramska and Petelski, 2003; Callaghan et al., 2008). Deliberate efforts in processing and analyzing photographic images of the sea state are required to separate the active part of the whitecaps and obtain W_A (Monahan and Woolf, 1989; Asher et al., 2002; Mironov and Dulov, 2008; Kleiss and Melville, 2010). The same is true for radiometric measurements of whitecap fraction. The basic principle of passive microwave measurement determines the outcome of radiometric observations to be the total whitecap fraction W (Anguelova and Webster, 2006; Anguelova

and Gaiser, 2011). An extensive database of W from satellites-based radiometric observations proves useful for studying and parameterizing the variability of whitecap fraction (Anguelova et al., 2010). However, to make such a database useful for dynamic processes in the upper ocean, it is necessary to find a way to extract W_A from W . This study describes our approach to build a database of W_A from available satellite-based observations of W .

2. ACTIVE WHITECAP FRACTION

2.1 Approaches to separate active whitecaps

We pursue the separation of W_A from W with two approaches. Physical basis of our theoretical approach is the Phillips concept of breaking wave statistics which connects active whitecap fraction W_A with the energy dissipation rate of breaking waves (Phillips, 1985). In this study we describe this approach (section 2.2) and present initial results (section 3).

Physical basis of our experimental approach is the distinct signature of active and residual whitecaps at infrared (IR) wavelengths (Marmorino and Smith, 2005). To this end, we conducted a multi-instrumental field campaign in April-May, 2012, on the Floating Instrument Platform (FLIP) drifting along the coast of California from Monterey Bay south toward Point Conception (Anguelova et al., 2012a). The instrumentation deployed includes sensors recording the whitecaps and breaking waves on the surface over wide range of the electromagnetic spectrum: visible (video cameras), infrared (IR camera), and microwave (radiometers at two frequencies, 10 GHz and 37 GHz). An acoustic array with three nested-aperture arrays at frequencies up to 2.4 kHz and aerosol/particle counter provide data for the bubbles generated beneath and sea spray produced above the whitecaps. Various auxiliary data such as wind speed, air temperature, humidity, wave field, and water temperature profile characterize the experimental conditions. We can use the IR data to identify a separation criterion which then can be applied to time series of microwave and acoustic data.

Having different physical bases, these two approaches can provide independent estimates of W_A on regional scales. Comparing results from the two approaches, we will be able to better understand, interpret, and constrain W_A values.

2.2 Theoretical approach

2.2.1 Phillips concept

Wind waves in the ocean break over a wide range of scales. It is important to be able to characterize the scale of a breaking wave because a small-scale breaker dissipates less energy than a breaking dominant wave. Phillips (1985) realized that the scale of a breaking wave may be partly represented by the length of the breaking crest Λ and its propagation velocity \bar{c} (visualized in Figure 1). Thus Phillips defined a statistical variable called breaking crest length distribution $\Lambda(\bar{c})d\bar{c}$ which shows the breaking length crests per unit area moving with velocity \bar{c} falling in the range from \bar{c} to $\bar{c} + d\bar{c}$.

Moments of the breaking crest length distribution define various statistics for breaking waves. Combining the first moment with the persistence time T of the bubbles, gives the active whitecap fraction:

$$W_A = \int_c Tc\Lambda(\bar{c})d\bar{c} \quad (1)$$

The fifth moment of the breaking crest length distributions determines the energy dissipation:

$$\varepsilon(\bar{c})d\bar{c} = bg^{-1}c^5\Lambda(\bar{c})d\bar{c} \quad (2)$$

where g is the acceleration due to gravity, and b is the so-called breaking parameter (Drazen et al., 2008). Expressing the first moment $c\Lambda(\bar{c})d\bar{c}$ via (2) and substituting it in (1), we obtain an expression for active whitecap fraction in terms of energy dissipation rate:

$$W_A(\varepsilon) = gTb^{-1} \int_c c^{-4} \varepsilon(\bar{c})d\bar{c} \quad (3)$$

In (3), term $\varepsilon(\bar{c})d\bar{c}$ can be presented with an expression for the spectral rate of energy loss from the wave components in the equilibrium range of the wave spectrum (Phillips, 1985, equation 6.6). Using such expression, we integrate (3) over suitable range of breaking front velocities (c_{min} , c_{max}). In the result of this integration, one can recognize an expression that can be obtained from the total (i.e., integrated) dissipation rate $\int_c \varepsilon(\bar{c})d\bar{c} = \langle \varepsilon \rangle / \rho_w$, where ρ_w is the density of seawater. Then for the active whitecap fraction we have:

$$W_A(\varepsilon) = \frac{gT}{4b\rho_w} \cdot \frac{\langle \varepsilon \rangle}{c_{min}^4 \cdot \ln(c_{max}/c_{min})} \quad (4)$$

Having this expression, one needs values for $\langle \varepsilon \rangle$, T , b , c_{min} , and c_{max} to obtain W_A . What is important in representing the active whitecap fraction with (4) is that

via c and $\langle \varepsilon \rangle$ the kinematic and dynamic of the breaking waves determine the values of W_A . That is, the active part is objectively separated from the residual, more static part of the whitecaps. From this point on, the challenge in obtaining reliable estimates of W_A is to obtain and/or choose well constrained values for the total dissipation rate and the various parameters in (4). The next two sub-sections describe our computation and choices for these quantities.

2.2.2 Total dissipation rate

Hanson and Phillips (1999) obtained total dissipation rate $\langle \varepsilon \rangle$ from measurements of wave spectra in the Gulf of Alaska following rigorously the equilibrium range model developed by Phillips (1985). Hwang and Sletten (2008) developed a parameterization for $\langle \varepsilon \rangle$ in terms of wind speed and wave characteristics:

$$\begin{aligned} \langle \varepsilon \rangle &= \alpha \rho_a U^3 \\ \alpha &= 0.2 \omega_*^{3.3} \eta_* \end{aligned} \quad (5)$$

where ρ_a is the air density, and the wave parameter α is determined using non-dimensional values for the frequency peak of the wave spectrum ω_* and surface elevation η_* . The results of this parameterization were validated with the $\langle \varepsilon \rangle$ values obtained by Hanson and Phillips (1999) and Felizardo and Melville (1995).

Whichever model one chooses to use to obtain $\langle \varepsilon \rangle$, it is important to use wave spectra of the wind seas and remove the swell. Hanson and Phillips (2001) remove the swell using the so-called topographic minima method. Hwang et al. (2012) develop the so-called spectrum integration method to remove the swell.

2.2.3 Parameter choices

There are four parameters in (4) whose values need to be chosen to obtain active whitecap fraction—the breaking parameter b , the bubble persistence T , the threshold breaker speed c_{min} , and the upper limit of the range of the breaker speeds c_{max} . We made a literature review for each of these parameters to find suitable measured and/or suggested values.

Table 1 summarizes the values reported in the literature for the breaking parameter b ; these are plotted in Figure 2. It is clearly seen that laboratory and field experiments, as well as modeling studies, give a wide range of possible values for b , from less than 0.1×10^{-3} to about 50×10^{-3} . We do not have a good physical justification at this moment to consider some values as more suitable than others. We thus use the average of all reported values $b = 0.0153$.

For the bubble persistence, we use a constant value $T = 2$ s. This value is the peak of the probability

density functions of whitecap lifetimes reported by Callaghan et al. (2012). Mueller and Veron (2009) justified the use of $T = \beta T_p$, where T_p is the dominant wave period at the peak of the wave spectrum. Coefficient β was chosen to be 0.2 so that their values of W_A match closely W_A data of Monahan (1993). Such a representation assumes noticeable influence of the wave field on the bubble persistence. We believe, however, that the wave field has weak, if any, effect on T , and factors like salinity, water temperature, and surfactants affect T much more. Because current knowledge of the effect of these quantities on T is missing, we opted for the constant value, which is based on photographic whitecap observations.

A host of values can be found in the literature for the threshold breaker speed c_{min} . Overall, it is usually suggested that c_{min} is somewhat less than the phase speed of the dominant wave c_p . Following Gemmrich et al. (2008), we obtain $c_{min} = \alpha_c c_p$ using $\alpha_c = 0.3$ which ensures values for c_{min} for breaking waves in fully developed sea. With data for T_p and c_p measured at buoy 41001, we obtain c_{min} in the range from 1.8 m s⁻¹ to 5.6 m s⁻¹. Others (Melville and Matusov, 2002; Banner and Peirson, 2007) suggest $\alpha_c \geq 0.8$. Such value, however, gives c_{min} too close to c_p and this places more emphasis on longer waves, which may break less frequently.

For the maximum value, we have chosen to use the ratio $c_{max}/c_{min} = 10$.

2.3 Extract active from total whitecap fraction

In this study, we use the parametric model of Hwang and Sletten (2008) to obtain $\langle \varepsilon \rangle$ from buoy data. Buoys that provide wind speeds and wave spectra were sought for these calculations. The wave spectra characteristics, namely peak wave period T_p and significant wave height H_s , were used to calculate the wave parameter α in (5). Swell is removed with the spectrum integration method (section 2.2.2).

Having $W_A(\varepsilon)$ values from buoy data, we then match-up those in time and space with W values from satellite-based (Windsat) radiometric observations. We thus are able to obtain a scaling factor $R = W_A/W$ on regional scale, i.e., around each buoy. The values of R at different buoy locations allow us to investigate the variability of this scaling factor in terms of wind speed and other meteorological and environmental factors.

The aim is to eventually develop a parameterization of R applicable for wide range of geographical locations and thus expand the regional R to a factor suitable on a global scale. This scaling factor can then be used together with global maps of W to obtain global maps of W_A and build a W_A database.

3. RESULTS

3.1 Data

We obtained active whitecap fraction values from energy dissipation rate $W_A(\varepsilon)$ using data from 5 buoys. Table 2 summarizes the locations, water depth, and climatology for each of these buoys. For all buoys, the wind speed values were converted from those at nominal 5-m reference height to U_{10} . Buoy data are 1-hour time series for the entire 2006. Figure 3 shows the positions of these buoys: four in Atlantic Ocean off the East coast of the USA, and one in the Gulf of Alaska. With these five buoys, we cover relatively wide range of geographical locations, from about 56° North to less than 30° N, and from about 73° West to 148° W.

Whitecap fraction W from WindSat measurements at 10 GHz and 37 GHz, horizontal polarization (hereafter denoted as 10H and 37H) are used. Figure 4 shows global monthly (March 2006) distribution of 10H W values (upper panel) and whitecap fraction obtained from $W(U_{10})$ parameterization (lower panel) (Monahan and O'Muirchaertaigh, 1980, hereafter MOM80). The spatial distributions have similar features but somewhat different magnitudes. The former is expected as satellite-based W values from 10H were found to be the closest to the photographically measured W values (Anguelova et al., 2009). The later points toward more uniform distribution of whitecap coverage from low to high latitudes, a finding which, though not as strongly expressed as in the feasibility study (Anguelova and Webster, 2006), is preserved in the W estimates used here and can be plausibly explained. Partially, it could be a consequence of still developing and improving performance of the retrieval algorithm. But it could also represent influences of the additional factors on the whitecapping.

In situ-satellite pairs of W_A and W were matched in time and space for the days when Windsat passes (ascending and descending) over each of the buoy locations were available. Spatially, we used all Windsat W estimates falling within a 0.5°×0.5° grid box around the location of each buoy. Then the W_A value from the buoy data closest in time to the time of the satellite overpass was taken and paired with the Windsat W value. For each buoy, we have up to about 150 W_A - W pairs for 2006 (see last column in Table 2).

3.2 Energy dissipation rate

This section illustrates the procedure to calculate W_A from data recorded at buoy 41001 (Figure 3 and Table 2). Figure 5a shows the wave parameter α for the case of nominal wave spectra values (i.e., mixed sea including swell, blue symbols), and for wind sea (i.e., swell removed, magenta symbols). The wind sea values for α compare favorably with a parameterization (red line) obtained from a different, independent dataset

(Hwang and Sletten, 2008). Figure 5b shows the total dissipation rate as a function of wind speed obtained with U_{10} and α for mixed and wind sea cases. The difference here from removing the swell is not significant, but for other buoys such a separation of the swell is needed.

Figure 6 (red symbols) shows the active whitecap fraction W_A obtained from the total dissipation rates in Figure 5 and the chosen parameters (section 2.2.3). These values are comparable in magnitude and wind speed dependence to W_A values obtained from previous photographic measurements (blue symbols). The figure also shows that W_A values could be up to 2 orders of magnitude lower than total W values (black symbols) also obtained from previous photographic observations. The line in the figure is the $W(U_{10})$ parameterization of MOM80 used also in Figure 4 (lower panel). Finally, the figure shows the total W values obtained from WindSat radiometric observations (10H and 37H) from which we want to extract W_A values. As their photographic counterpart (and as expected), these total W values are larger than the $W_A(\varepsilon)$.

We have performed a sensitivity study for the effect of the parameter choices on the obtained $W_A(\varepsilon)$ values. An increase of the persistence of bubbles T leads to an increase of the $W_A(\varepsilon)$ values. This could be expected as larger T values suggest long-lived, thus decaying, foam which covers larger area (section 1). Increasing the threshold breaker speed c_{min} , we obtain lower $W_A(\varepsilon)$ values. This is physically plausible as faster waves are also longer and they might not break as they might have reached equilibrium with the wind input. Finally, higher values of the breaking parameter b give lower $W_A(\varepsilon)$ values. While this observation is not readily interpretable, we found that the choice of the breaking parameter value has the largest effect on the calculated $W_A(\varepsilon)$ values. Thus tuning of the procedure to obtain well constrained $W_A(\varepsilon)$ values must start with a better understanding of the nature and reasonable choice of the value of parameter b .

3.3 Active whitecap fraction and scaling factor

Figure 7 shows the $W_A(\varepsilon)$ values for all 5 buoys obtained with the chosen parameters (section 2.2.3). Photographic W and W_A values and the $W(U_{10})$ parameterization are also included for reference. The panels show the change of the $W_A(\varepsilon)$ values from higher latitudes to lower. As the figures shows, moving toward lower latitudes, we observe ever increasing $W_A(\varepsilon)$ values.

What causes these changes is not easy to pinpoint at this moment. As the climatology of the buoy locations shows (Table 2), the conditions change in different pace from the location of buoy 46001 in the Gulf of Alaska to

that of buoy 41010. The water temperature changes by 72% from its maximum of 25.6 °C at buoy 41010 to 7.1 °C at buoy 46001. Meanwhile the wind speed changes by only 26% from its maximum value of 9.2 m s⁻¹ to its minimum of 6.8 m s⁻¹. The changes in the wave field (quantifies with H_s or wave slope $\sim H_s/T_p^2$) is even less telling. More in situ-satellite pairs over wider geographical range are necessary in order to understand the variations of $W_A(\varepsilon)$ with the wind speed and other factors.

Though we realize the need for more data, here we show first results for the scaling factor $R = W_A(\varepsilon)/W$ as a function of wind speed (Figure 8). In panel a, we show R for all available in situ-satellite pairs at buoy 41001. Plotted in the figure are scaling factors associated with satellite-based values W at 10H (green symbols) and 37H (magenta symbols). We also give R obtained from $W_A(\varepsilon)$ and $W(U_{10})$ parameterization of MOM80 (red symbols). As the figure shows, there is no distinct difference between these three sets of values. Also, there is no discernible dependence on wind speed up to about $U_{10} = 7$ m s⁻¹. For higher winds, the correlation between R and U_{10} is somewhat tighter.

Figure 8b compares the scaling factors R from the five buoys. Plotted are binned values for R in wind speed bins with width of 1 m s⁻¹. This figure shows that there is something like a peak of $R(U_{10})$ about 7 m s⁻¹ wind, with R values lower than this peak for winds below and above 7 m s⁻¹. As for the differences between buoys, i.e., geographical locations, there is a discernible trend of R being lower in colder waters (magenta stars for buoy 46001) and increasing in warmer waters (blue squares for buoy 41012).

4. CONCLUSIONS

We have compiled a database of whitecap fraction W from satellites-based microwave radiometric observations. These observations provide the total W including foam generated during active breaking of wind-driven waves and residual foam left behind by these breaking waves. Predictions of sea spray aerosol production and heat exchange use values of W . However, the whitecap fraction associated with the actively breaking waves W_A is needed for dynamic air-sea processes in the upper ocean such as turbulent mixing, gas exchange, ocean ambient noise, and spray-mediated intensification of tropical storms. To parameterize such processes, a database of W_A separate from W is needed.

Here we demonstrate that such a separation is feasible by combining the Phillips concept of breaking wave statistics which connects W_A with the energy dissipation rate of breaking waves ε and parametric

estimates of total energy dissipation rate $\langle \varepsilon \rangle$ from wave spectra measured from buoys. We describe the principle of the W versus W_A separation, identify the parameters that affect the accuracy of our approach, and present results for a scaling factor between W_A and W .

5. REFERENCES

Andreas, E.L., P.P.G. Persson, J.E. Hare, 2008: A bulk turbulent air-sea flux algorithm for high-wind, spray conditions. *J. Phys. Oceanogr.*, **38**, 1581-1596, doi:10.1175/2007JPO3813.1.

Anguelova, M. D. , M. Bettenhausen, W. Johnston, P. Gaiser, 2010: First extensive whitecap database and its use to study whitecap fraction variability, 17th Air-Sea Interaction Conference, AMS, 26 - 30 September, Annapolis, MD (ams.confex.com/ams/17Air17Sat9Coas/techprogram/paper_174036.htm).

Anguelova, M. D., J. P. Bobak, W. E. Asher, D. J. Dowgiallo, B. I. Moat, R. W. Pascal, and M. J. Yelland, 2009: Validation of satellite-based estimates of whitecap coverage: Approaches and initial results, 16th Air-Sea Interaction conference, AMS, 10-15 January, Phoenix, Arizona. (ams.confex.com/ams/89annual/techprogram/paper_143665.htm).

Anguelova, M.D., D. J. Dowgiallo, G. Smith, S. L. Means, I. B. Savelyev, G. M. Frick, C. M. Snow, J. A. Schindall, and J. P. Bobak, 2012a: The many faces of oceanic whitecaps: A multi-instrument field campaign, Poster # 63, 18th Air-Sea Interaction Conference, AMS, 9-12 July, Boston, MA, USA. (ams.confex.com/ams/20BLT18AirSea/webprogram/Paper209180.html).

Anguelova, M. D., and P. W. Gaiser, 2011: Skin depth at microwave frequencies of sea foam layers with vertical profile of void fraction. *J. Geophys Res.*, **116**, C11002, doi:10.1029/2011JC007372

Anguelova, M.D., and F. Webster, 2006: Whitecap coverage from satellite measurements: A first step toward modeling the variability of oceanic whitecaps. *J. Geophys. Res.-Oceans*, **111**, C03017, doi:10.1029/2005JC003158.

Asher, W. Wang, Q. Monahan, E. C. Smith, P. M., 1998: Estimation of Air-Sea Gas Transfer Velocities from Apparent Microwave Brightness Temperature. *J. Mar. Tech. Soc.*, **32**, 32-40.

Asher, W.E., J. B. Edson, W. R. McGillis, R. Wanninkhof, D. T. Ho, and T. Litchendorf, 2002: Fractional area whitecap coverage and air-sea gas transfer velocities measured during GasEx-98, in *Gas Transfer at Water Surfaces*, **127**, Geophysical Monograph, M. A. Donelan, W. M. Drennan, E. S. Saltzman, and R. Wanninkhof, Eds. Washington, DC, AGU, 199-204.

Babanin, Alexander V., Kakha N. Tsagareli, I. R. Young, David J. Walker, 2010: Numerical Investigation of Spectral Evolution of Wind Waves. Part II: Dissipation Term and Evolution Tests. *J. Phys. Oceanogr.*, **40**, 667-683.

Banner, M.L., and W.L. Peirson, 2007: Wave breaking onset and strength for twodimensional deepwater wave groups. *J. Fluid Mech.*, **585**, 93115 doi:10.1017/S0022112007006568

Callaghan, A. H., G. de Leeuw, L. Cohen, and C. D. O'Dowd, 2008: Relationship of oceanic whitecap coverage to wind speed and wind history. *Geophys. Res. Lett.*, **35**, L23609, doi:10.1029/2008GL036165.

Callaghan, A. H., G. Deane, M. D. Stokes, and B. Ward, 2012: Observed Variation in the Decay Time of Oceanic Whitecap Foam. *J. Geophys. Res.*, doi:10.1029/2012JC008147, in press (www.agu.org/pubs/crossref/pip/2012JC008147.shtml).

de Leeuw, G., E. Andreas, M. D. Anguelova, C. Fairall, E. Lewis, C. O'Dowd, M. Schulz, S. Schwartz, 2011: Production Flux of Sea-Spray Aerosol. *Rev. Geophys.*, **49**, RG2001, doi:10.1029/2010RG000349.

Deane, G. B., and M. D. Stokes, 2002: Scale dependence of bubble creation mechanisms in breaking waves. *Nature*, **418**, 839-844.

Drazen, D. A., W. K. Melville, and Luc Lenain, 2008: Inertial scaling of dissipation in unsteady breaking waves. *J. Fluid Mech.*, **611**, 307332, doi:10.1017/S0022112008002826

Duncan, J. H., 1981: An experimental investigation of breaking waves produced by a towed hydrofoil. *Proc. R. Soc. Lond. A*, **377**, 331-348.

Duncan, J. H., 1983: The breaking and non-breaking wave resistance of a two-dimensional hydrofoil. *J. Fluid Mech.*, **126**, 507-520.

Felizardo, F. C., and W. K. Melville, 1995: Correlations between Ambient Noise and the Ocean Surface-Wave Field. *J Phys Oceanogr*, **25**, 513-532.

Gemmrich, J. R., M. L. Banner, and C. Garrett, 2008: Spectrally resolved energy dissipation rate and momentum flux of breaking waves. *J Phys Oceanogr*, **38**, 1296-1312.

Hanson, J. L., and O. M. Phillips, 1999: Wind sea growth and dissipation in the open ocean. *J Phys Oceanogr*, **29**, 1633-1648.

Hanson, J. L., and O. M. Phillips, 2001: Automated analysis of ocean surface directional wave spectra. *J Atmos Ocean Tech*, **18**, 277-293.

Hwang, P. A., and M. A. Sletten, 2008: Energy dissipation of wind-generated waves and whitecap coverage. *J. Geophys. Res.*, **113**, C02012, doi:10.1029/2007JC004277.

Hwang, Paul A., Francisco J. Ocampo-Torres, Héctor García-Nava, 2012: Wind Sea and Swell Separation of

1D Wave Spectrum by a Spectrum Integration Method. *J. Atmos. Oceanic Technol.*, **29**, 116–128.

Iafrazi, A., 2011: Energy dissipation mechanisms in wave breaking processes: Spilling and highly aerated plunging breaking events. *J. Geophys. Res.*, **116**, C07024, doi:10.1029/2011JC007038.

Kleiss, J. M., and W. K. Melville, 2010: Observations of Wave Breaking Kinematics in Fetch-Limited Seas. *J. Phys. Oceanogr.*, **40**, 2575–2604, doi: http://dx.doi.org/10.1175/2010JPO4383.1

Marmorino, G. O., and G. B. Smith, 2005: Bright and dark ocean whitecaps observed in the infrared. *Geophys. Res. Lett.*, **32**, L11604, doi:10.1029/2005GL023176

Melville, W.K., 1994: Energy-Dissipation by Breaking Waves. *J Phys Oceanogr*, **24**, 2041-2049.

Melville, W.K., 1996: The role of surface-wave breaking in air-sea interaction. *Annu. Rev.Fluid Mech.*, **28**, 279-321.

Melville, W. K., and P. Matusov, 2002: Distribution of breaking waves at the ocean surface. *Nature*, **417**, 58-63.

Melville, W. K., F. Veron, and C. J. White, 2002: The velocity field under breaking waves: coherent structures and turbulence. *J Fluid Mech*, **454**, 203-233.

Mironov, A. S., and V.A. Dulov, 2008: Detection of wave breaking using sea surface video records. *Meas. Sci. Technol.* **19** 015405.

Monahan, E., and I. G. O'Muircheartaigh, 1980: Optimal power-law description of oceanic whitecap coverage dependence on wind speed. *J. Phys. Oceanogr.*, **10**, 2094–2099.

Monahan, E. C., C. W. Fairall, K. L. Davidson, and P. J. Boyle, 1983: Observed Interrelations between 10m Winds, Ocean Whitecaps and Marine Aerosols. *Q J Roy Meteor Soc*, **109**, 379-392.

Monahan, E., and D. K. Woolf, 1989: Comments on "Variations of whitecap coverage with wind stress and water temperature." *J. Phys. Oceanogr.*, **19**, 706-709.

Monahan, E. C., 1993: Occurrence and evolution of acoustically relevant subsurface bubble plumes and their associated, remotely monitorable, surface whitecaps. *Natural Physical Sources of Underwater Sound*, B. R. Kerman, Ed., Kluwer, 503–517.

Mueller, J. A., F. Veron, 2009: A Sea State–Dependent Spume Generation Function. *J. Phys. Oceanogr.*, **39**, 2363–2372, doi: ttp://dx.doi.org/10.1175/2009JPO4113.1

Phillips, O. M., 1985: Spectral and Statistical Properties of the Equilibrium Range in Wind-Generated Gravity-Waves. *J Fluid Mech*, **156**, 505-531.

Phillips, O. M., F. L. Posner, and J. P. Hansen, 2001: High range resolution radar measurements of the speed distribution of breaking events in wind-generated ocean

waves: Surface impulse and wave energy dissipation rates. *J Phys Oceanogr*, **31**, 450-460.

Stramska, M., and T. Petelski, 2003: Observations of oceanic whitecaps in the north polar waters of the Atlantic. *J. Geophys. Res.*, **108**(C3), 3086, doi:10.1029/2002JC001321

Thomson, J., J. R. Gemmrich, and A. T. Jessup, 2009: Energy dissipation and the spectral distribution of whitecaps. *Geophys Res Lett*, **36**.

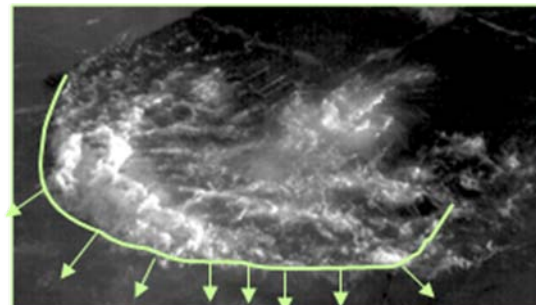


Figure 1 Visualization of breaking crest length Δ and breaker speed velocity \bar{c} (green curve and arrows overlaid on a breaking wave). Photo courtesy: Bill Asher.

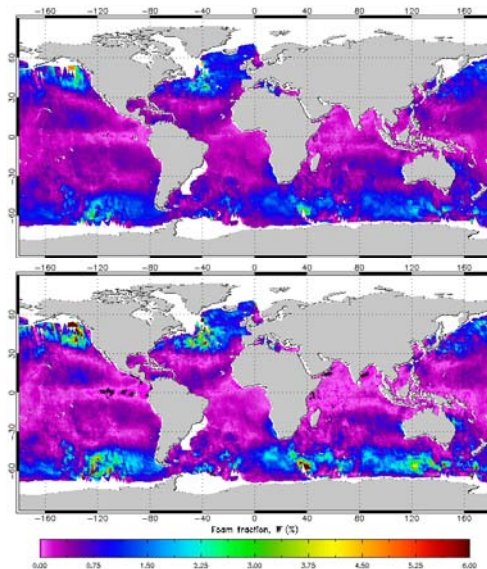


Figure 4 Global monthly (March, 2006) distribution of whitecap coverage from WindSat measurements at 10 GHz, H pol. (10H, upper panel) and $W(U_{10})$ model of Monahan and O'Muircheartaigh (1980) (lower panel).

TABLE 1Summary of values of breaking parameter b reported in the literature.

Value #	Reference	$b \times 10^3$	Notes
1	Duncan (1981)	44 ± 8	Quasi-steady breaking
2	Duncan (1983)	32 to 75	Quasi-steady breaking
3	Melville (1994)	4 to 12	Unsteady, Lowen (1991) data
4	Melville (1994)	3 to 16	Unsteady, scaling arguments
5	Phillips et al. (2001)	0.7 to 1	Radar field measurements
6	Deane&Stokes (2002)	8.6	Unsteady, lab bubble data
7	Melville et al. (2002)	7	Unsteady, lab measurements
8	Banner&Peirson (2007)	0.08 to 1.2	Lab measurements
9	Gemrich et al. (2008)	0.032 to 0.101	$\mathcal{A}(c)$ from video, FLIP
10	Drazen et al. (2008)	3 to 63	Lab data (Fig. 11), $b=0.31S^{2.77}$
11	Thomson et al. (2009)	17 ± 30	Lake measurements
12	Thomson et al. (2009)	13 ± 50	Indirect estimate
13	Iafrafi (2011)	8 to 11	Model (Fig. 7 and eq. 16)
14	Babanin et al. (2010)	0.001 to 10	Model (Fig. 11 and eq. 24)
	Mean value	15.3	

TABLE 2

Summary of buoy locations and climatology. See the text for definition of the symbols.

Buoy ID	Lon W	Lat N	SST °C	$U_{10} \text{ ms}^{-1}$	$T_p \text{ s}$	$H_s \text{ m}$	$s = H_s / T_p^2$	Depth m	W_A - W pairs
46001	148.02	56.3	7.13	6.8	8.18	2.26	0.021644	4206	36
41001	34.7	34.7	22.6	8.5	7.26	2.01	0.024437	4462.3	123
41002	32.31	32.31	23.9	9.2	6.92	1.6	0.021411	3474.7	161
41012	80.53	30.04	23.7	7.1	5.47	0.92	0.019704	38.1	156
41010	28.91	28.91	25.6	7.9	6.45	1.3	0.020024	872.6	178

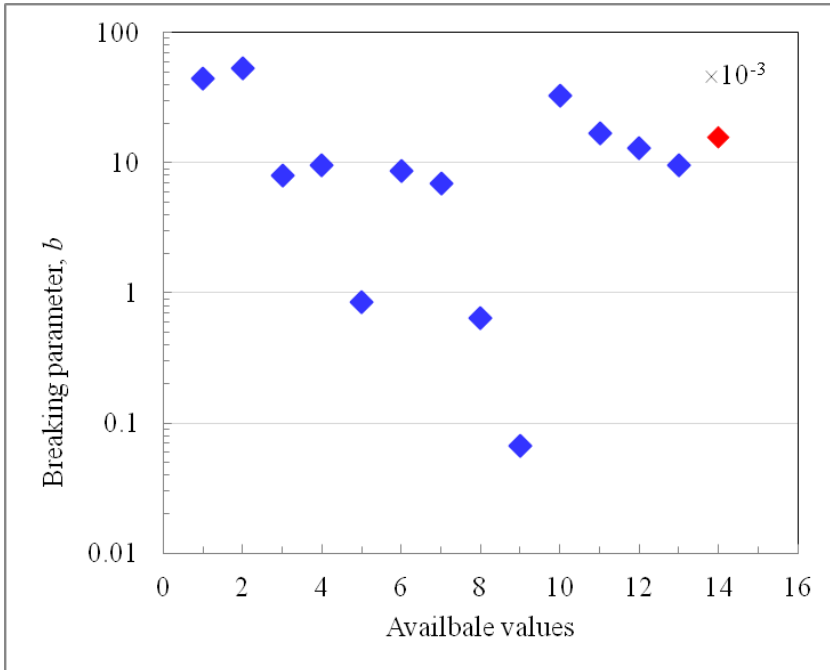


Figure 2 Available values of breaking parameter b . See also Table 1.

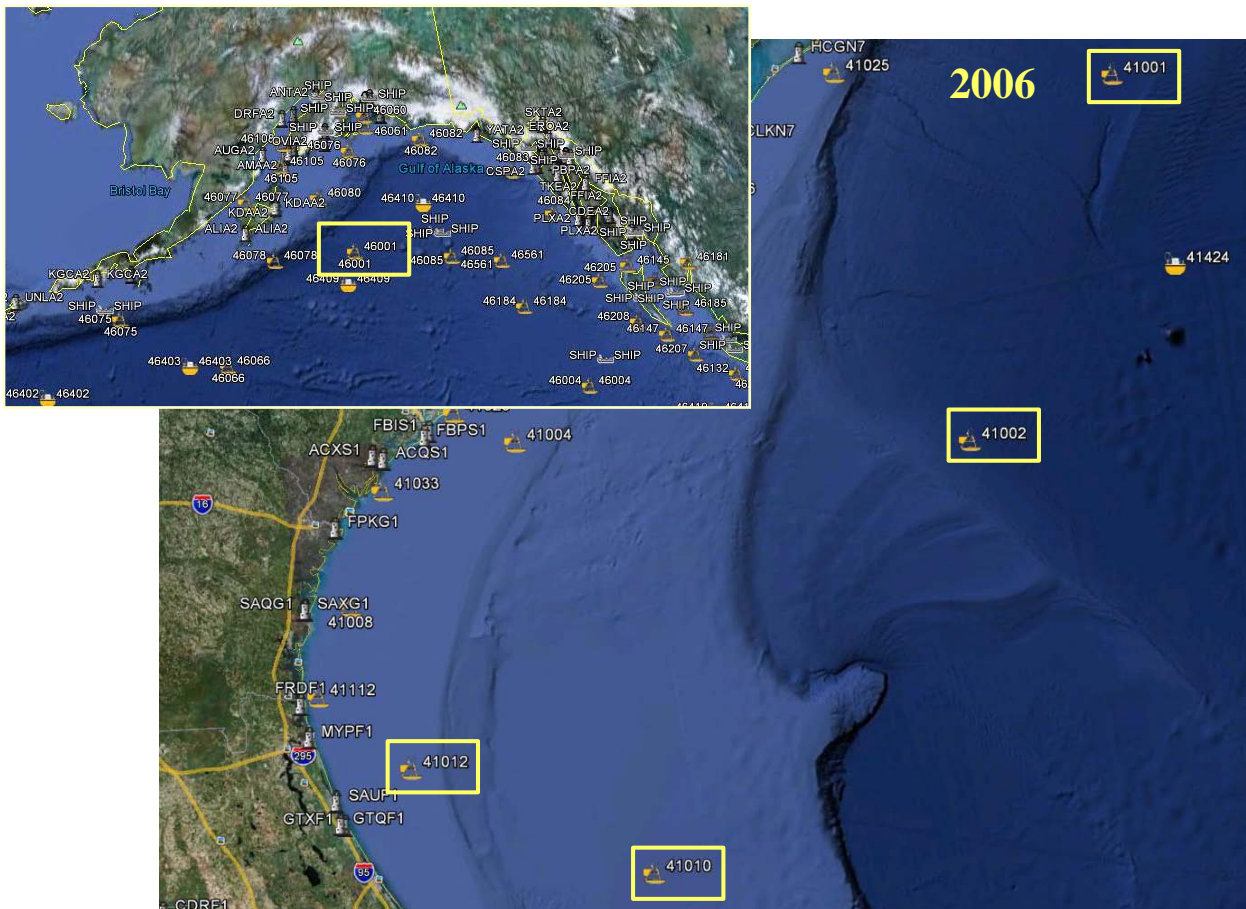


Figure 3 Locations of 5 buoys used to calculate total dissipation rate $\langle \epsilon \rangle$ and active whitecap fraction W_A

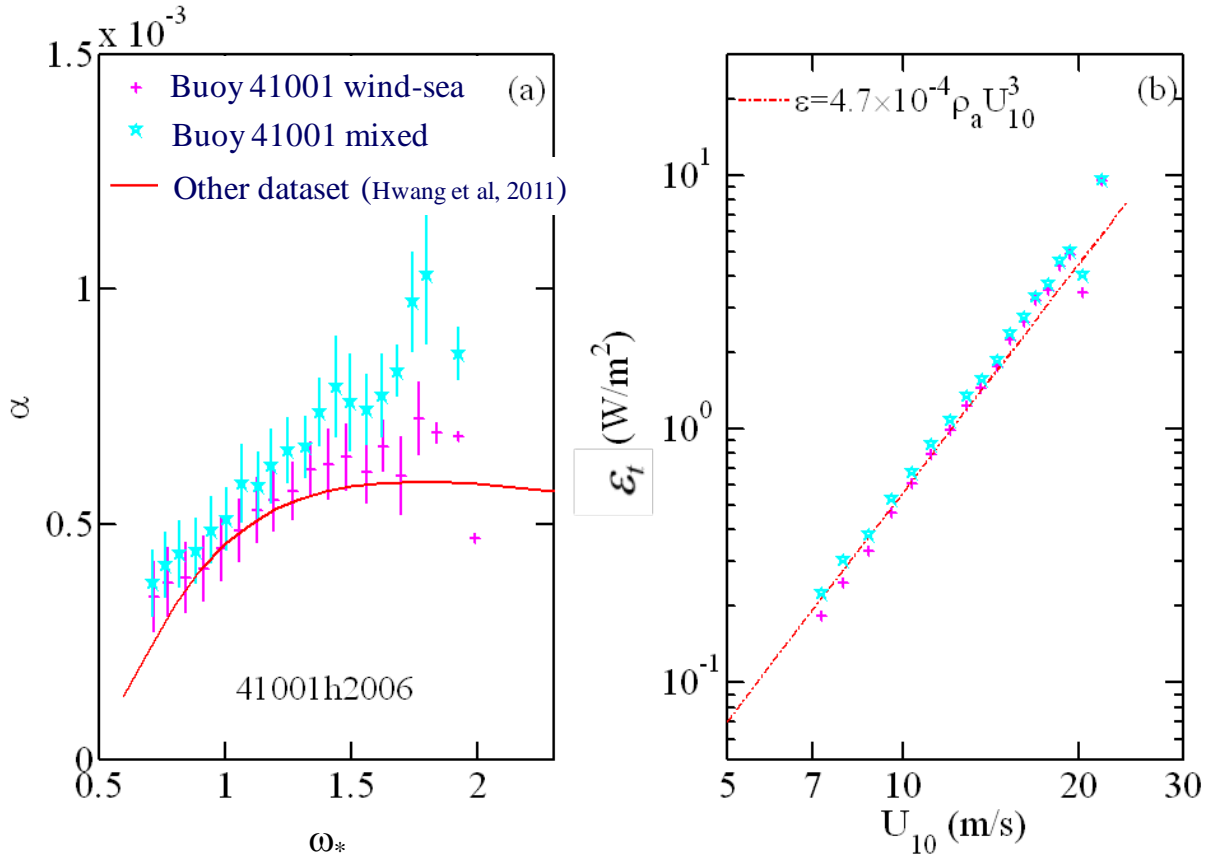


Figure 5 a) Wave parameter α from data measured at buoy 41001. b) Total dissipation rate $\langle \epsilon \rangle$. Blue symbols are for mixed sea (wind waves and swell); magenta symbols are for wind seas (swell removed); red lines are parameterizations.

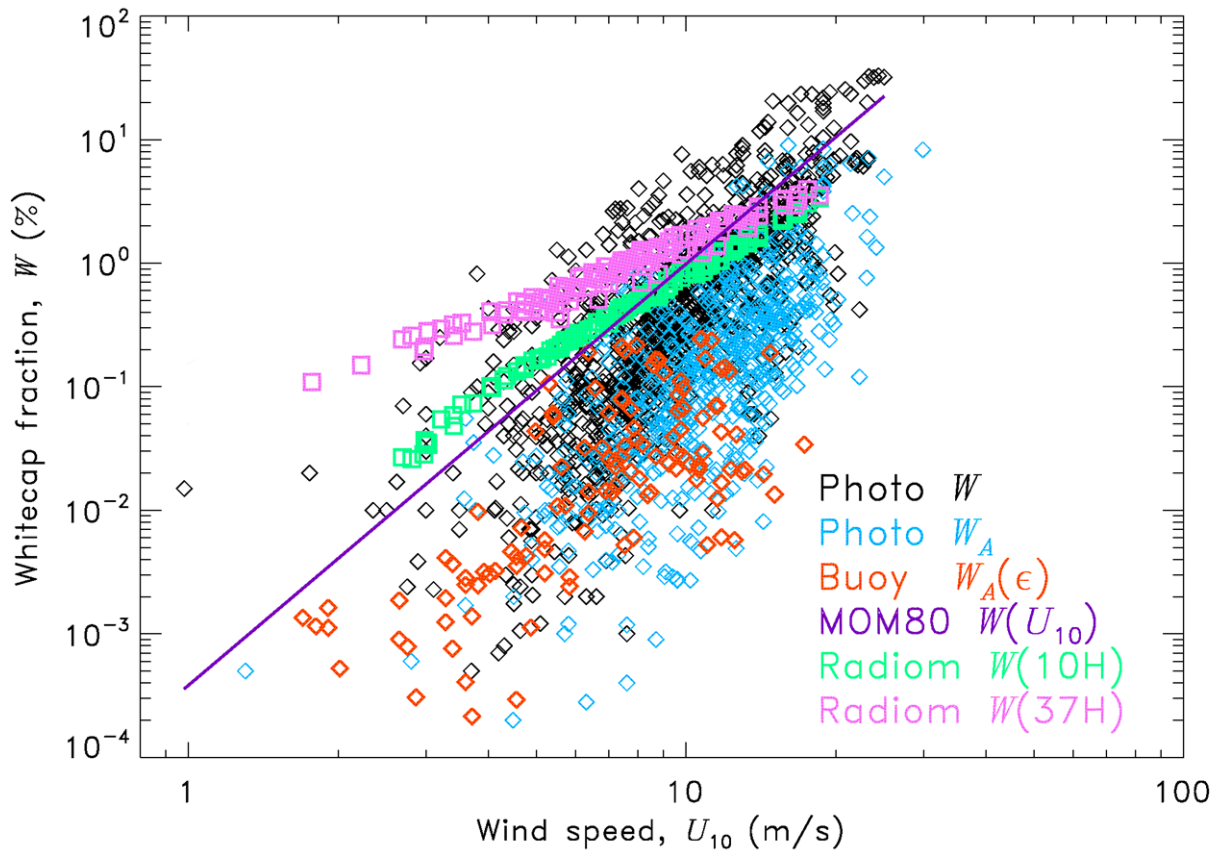
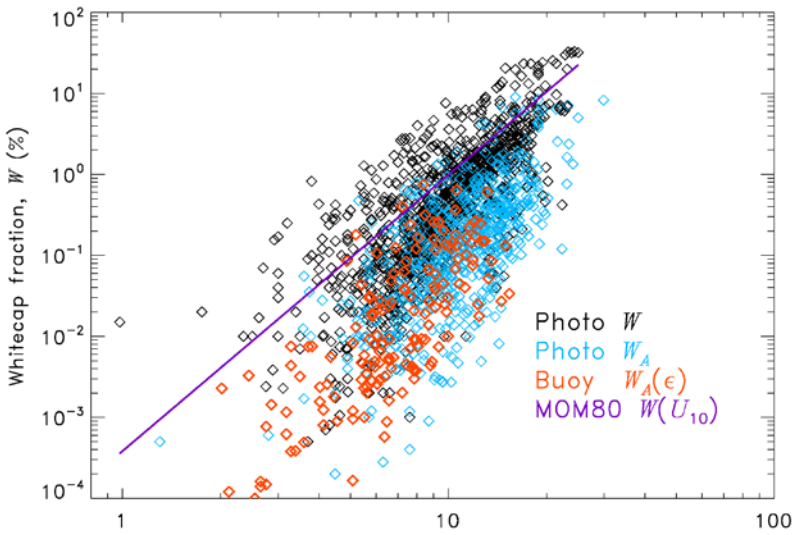
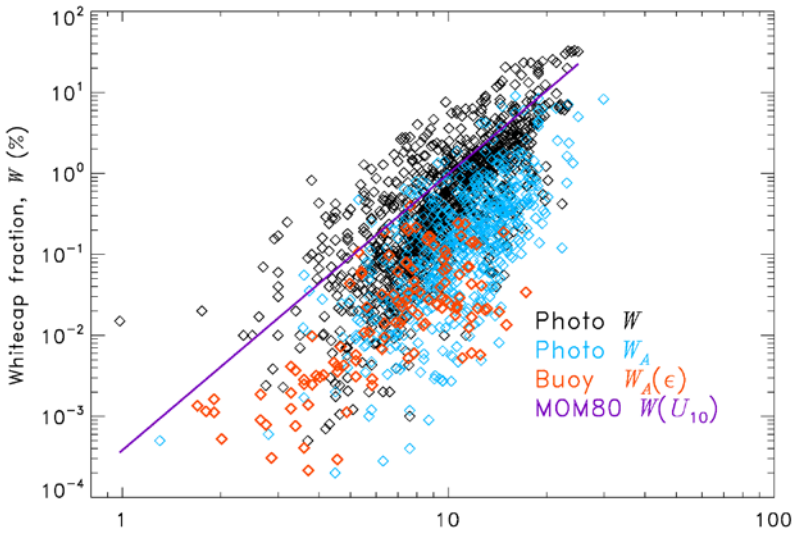
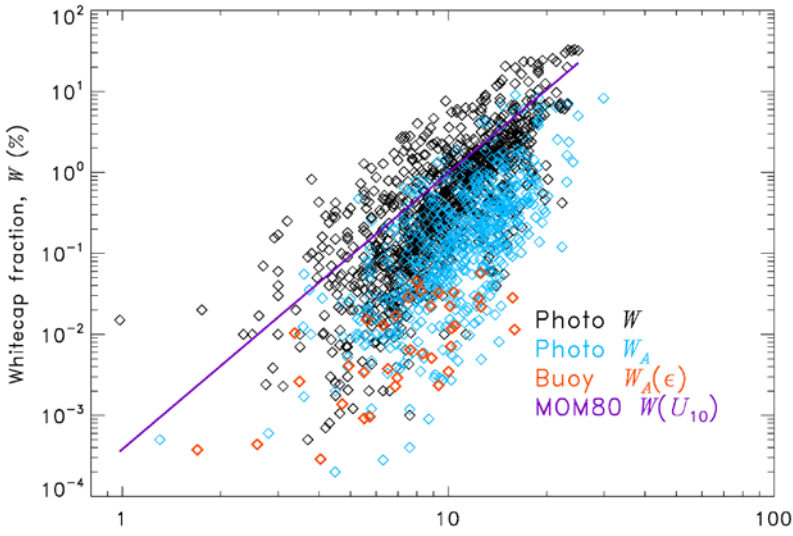


Figure 6 Active whitecap fraction obtained from energy dissipation rate for buoy 41001.



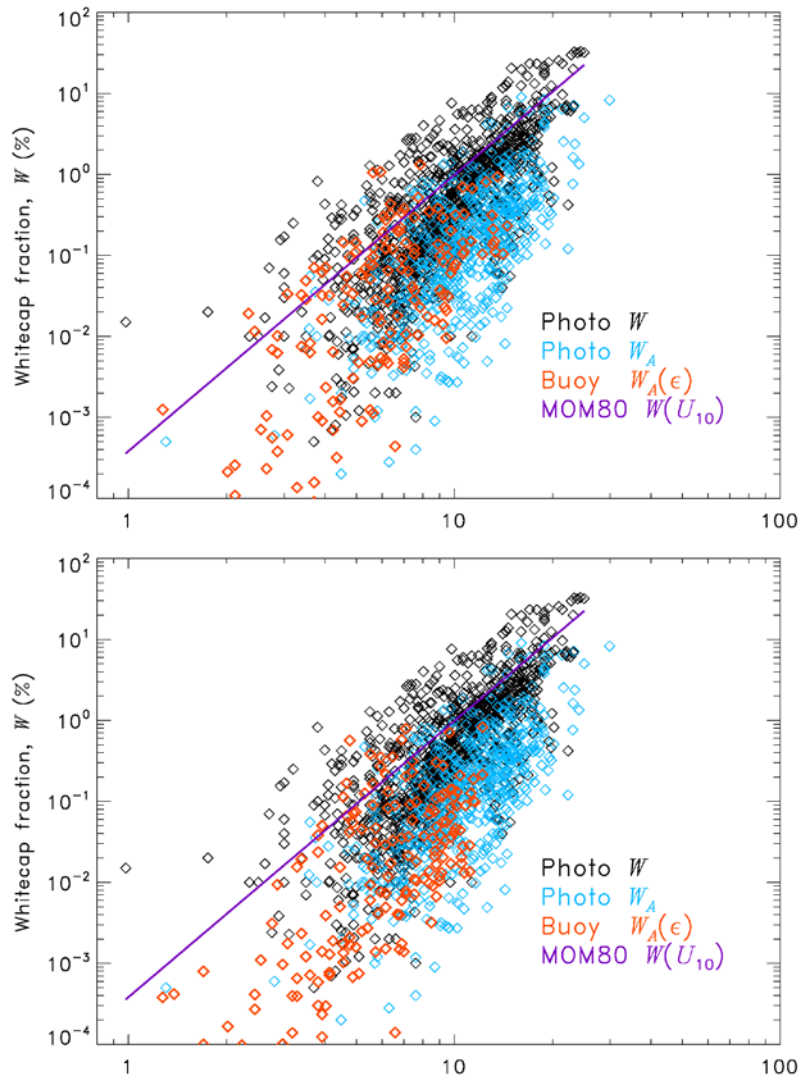


Figure 7 Comparison of W_A values from photographic measurements (blue symbols) and energy dissipation calculations (red symbols) for all buoys (from top down: 46001, 41001, 41002, 41012, 41010).

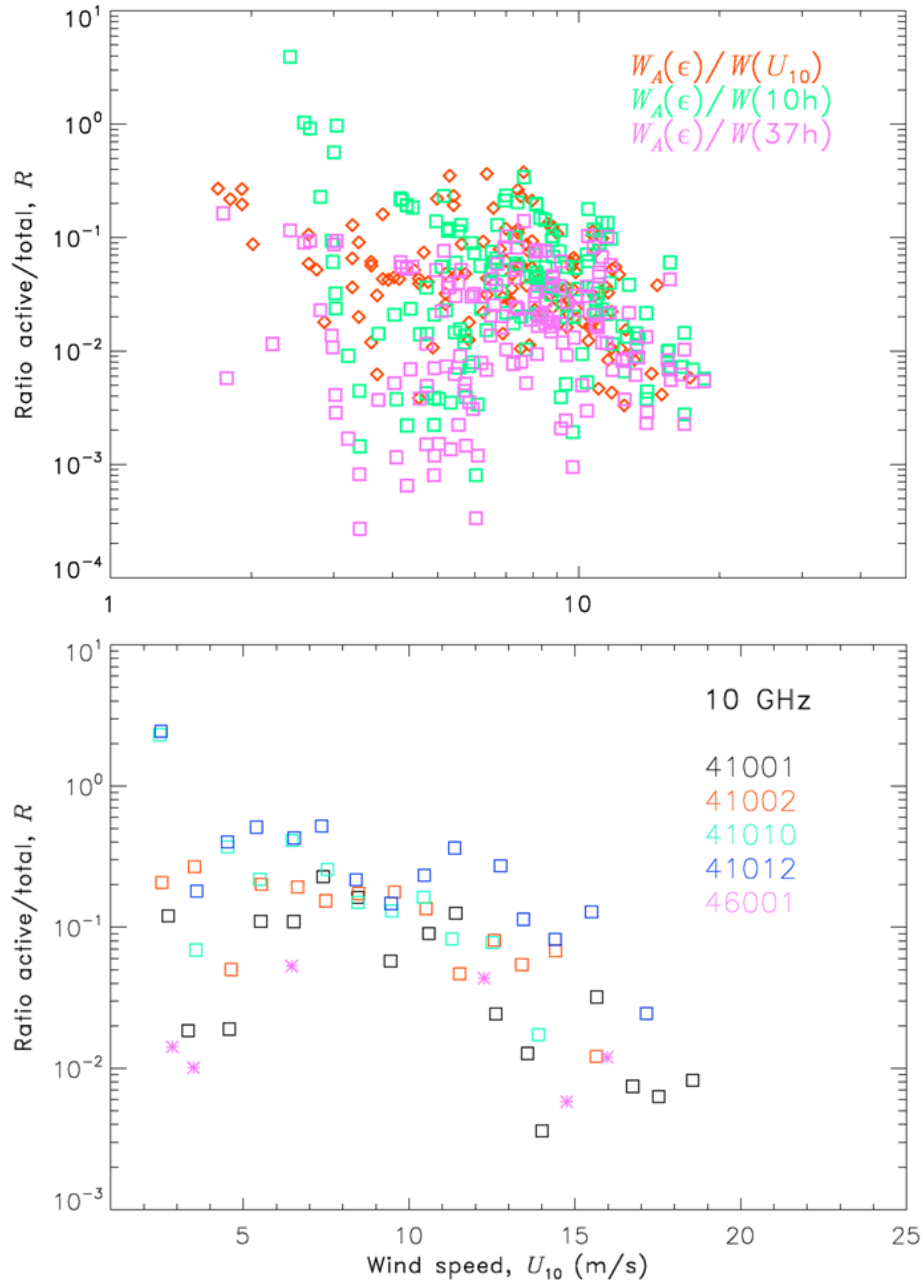


Figure 8 Scaling factor $R = W_A/W$ as a function of wind speed: a) All available values for buoy 41001; b) Comparison of R for all buoys; R values are binned by wind speed in bins of 1 m s^{-1} width.